scientific reports

Check for updates

OPEN

Effects of thermal aging on the performance of ordinary and novel superhydrophobic and oleophobic ultra-fine dry powder extinguishing agent

Yurong Liu[1,2], Ruiyu Chen[2]✉, Wang Zhixuan[2], Rui Zhang[3], Hongling Jing[3], Daheng Yu[3] & Renming Pan[2]✉

Powder-based fire extinguishing agents have become a kind of promising substitutes for halon extinguishing agents in civil aircrafts. However, their storage lifespan, significantly influenced by the thermal aging, emerges as a crucial yet overlooked aspect for aviation use. This study investigates the effects of thermal aging cycles on various parameters of ordinary dry powder extinguishing agent (ODPEA) and novel superhydrophobic and oleophobic ultra-fine dry powder extinguishing agent (SHOU DPEA), including surface microscopic morphology, D90 (the diameter at which 90% of the cumulative volume of particles are equal to or smaller than this value), chemical structure, hydrophobic and oleophobic angles, flowability, extinguishing time and effectiveness. The results indicate that SHOU DPEA exhibits smaller particle size, more regular particle shape, significantly superior heat stability and flowability compared to ODPEA. Furthermore, the D90 value evolution of ODPEA with aging time exhibits two stages: (a) a slow and linear growth stage (0–160 days), and (b) a rapid and substantial growth stage (160–200 days). However, SHOU DPEA shows a gradual increase in D90 value throughout the entire accelerated aging process. After 160 days of aging or more, the performance of ODPEA has significantly deteriorated, while SHOU DPEA has shown less degradation. Specially, the extinguishing concentration for the 160-day-aged ODPEA exceeds that of non-aged ODPEA by 10%, whereas the concentration of the 200-day-aged SHOU DPEA is less than 10% of the non-aged counterpart. Additionally, the predicted lifespans for ODPEA and SHOU DPEA at room temperature (25 °C) are 2715 days and over 4525 days, respectively. These findings can provide valuable guidance for assessments and the selection of aviation fire extinguishing agents.

Keywords Predicted storage lifespan, Ultra-fine dry powder extinguishing agent, Aviation firefighting, Superhydrophobic and oleophobic

Halon fire extinguishing agents have been extensively utilized in aviation firefighting due to their exceptional performance, such as high extinguishing efficiency, residue-free application, and lightweight characteristics. However, their harmful impact on the atmospheric ozone layer has prompted international action to restrict their production and use[1]. Early substitutes, such as halogenated hydrocarbons (e.g., CF_2Br_2[2]), provided similar firefighting capabilities but still contributed to ozone depletion. This has driven researchers to seek more environmentally friendly alternatives aligned with global sustainability goals.

Inert gases, including nitrogen (N_2), carbon dioxide (CO_2), and IG-541, emerged as environmentally friendly substitutes for Halon, as they do not deplete the ozone layer[3]. However, these gases necessitate higher pressures and larger storage containers to achieve comparable firefighting effectiveness, which presents engineering challenges in aviation applications. In contrast, powder-based fire extinguishing agents[4–10] have gained increasing attention in recent years due to their high extinguishing efficiency, excellent total flooding

[1]State Key Laboratory of Precision Blasting, Jianghan University, Wuhan, Hubei, People's Republic of China. [2]School of Safety Science and Engineering (School of Emergency Management), Nanjing University of Science and Technology, Nanjing 210094, People's Republic of China. [3]Tianjin Aviation Electro-Mechanical Co., Ltd, Tianjin 300300, China. ✉email: crynjust@njust.edu.cn; panrenming@njust.edu.cn

capabilities, and environmentally benign characteristics, including low toxicity and ozone layer preservation. Therefore, fire extinguishing vehicles equipped with ordinary dry powder extinguishing agents (ODPEAs) and ultra-fine dry powder extinguishing agents (UDPEAs) are widely utilized on airport runways, aprons, cargo areas, etc. The development of these agents not only meets the demand for efficient firefighting solutions but also aligns with environmental conservation objectives.

Of particular interest are ultra-fine dry powder extinguishing agents (UDPEAs), which are currently under investigation for their thermal decomposition characteristics, extinguishing efficiency, and resistance to re-ignition. Researchers have particularly focused on surface modification techniques to enhance the hydrophobic and oleophobic properties[11–13] of these powders, which improves their extinguishing performance and long-term storage stability. For example, Ning et al.[14] modified sodium bicarbonate UDPEA using a copolymer of silicone oil and perfluorohexyl acrylate (FP), obtaining superhydrophobic and oleophobic ultra-fine dry powder extinguishing agent (SHOU DPEA). Building upon Ning's work, Liu et al.[15] further investigated the thermal decomposition characteristics, kinetics, volatile products, reaction models, and chemical reaction mechanisms of SHOU DPEA using thermal analysis[16]. Zhao et al.[12] prepared modified ammonium polyphosphate UDPEA with superhydrophobic, superoleophobic, and high chemical activity. Its aviation kerosene repellency exceeded 98%, demonstrating excellent re-ignition resistance. Zhao et al.[17] studied the fire extinguishing efficiency of ammonium phosphate UDPEA under different pressures, revealing that the fire extinguishing efficiency of UDPEA increases with pressure. In summary, the hydrophobicity and oleophobicity of UDPEAs play a crucial role in enhancing their firefighting effectiveness and resistance to re-ignition.

It is worth noting that the practical application of UDPEA in aircraft requires consideration of the demands of actual engineering applications, such as storage life. Currently, the fire extinguishing agents used in aircraft are homogeneous and stable gaseous halon fire suppressants, which eliminates any concerns regarding storage life. In contrast, during long-term storage, UDPEAs may experience diminished effectiveness for the following reasons: (1) Due to its small particle size and larger specific surface area, it is more susceptible to agglomeration and reduced flowability when exposed to moisture. (2) Slow decomposition of active components resulting in decreased fire extinguishing efficiency. (3) The failure of the hydrophobic and oleophobic layers on the surface of the fire extinguishing agent resulting in the loss of resistance against re-ignition.

The International Civil Aviation Organization (ICAO) does not explicitly specify the usage lifespan for UDPEAs. However, it recommends that countries and regions establish corresponding regulations for the usage lifespan based on specific circumstances[18]. For instance, the United States Federal Aviation Administration (FAA) mandates a comprehensive inspection and maintenance of UDPEAs every five years. In 2017, South Korea enacted the "Enforcement Decree of the Fire Safety Act," which introduced a 10-year usage limit for fire extinguishers[19]. Nevertheless, there currently needs to be a clear legal standard for assessing the lifespan of UDPEAs. The Russian GOST 26592-86 NPB 170-98 recommends evaluating the fire extinguishing efficiency and flowability of the powder as the crucial indicators for assessing the storage life of fire extinguishing agents[20]. Kim et al.[21] analyzed physical characteristics such as moisture content, hygroscopicity, penetration depth, bulk density, and particle size through accelerated thermal aging experiments. The research indicates that these physical features are insufficient to determine the endpoint of failure. They suggest that further in-depth academic studies are needed in the future to establish usage standards for ABC class fire extinguishing agents.

The effects of thermal aging[22] on the performance of ODPEA and novel SHOU DPEA are comprehensively and quantitatively investigated in the present study. ODPEA is considered for that it has been widely used as the fire extinguishing agent in ground-based aviation area and the comparison of performance of ODPEA and SHOU DPEA can provide useful information for the application of SHOU DPEA in aircrafts. Therefore, the significance of this study lies in exploring the challenges of UDPEA in practical aircraft applications and proposing solutions, while also conducting a comprehensive comparison and evaluation of different types of fire extinguishing agents, providing important references for improving aircraft fire extinguishing efficiency and safety. In the current study, we conduct a continuous 200-day accelerated thermal aging experiment on the two fire extinguishing agents. The evolution of their surface morphology is observed using scanning electron microscopy (SEM). Instrumentation such as a laser intensity tester, contact angle measurement device, Fourier-transform infrared spectrometer (FTIR), and powder bulk density analyzer are used to characterize the D90 (the diameter at which 90% of the cumulative volume of particles are equal to or smaller than this value), hydrophobic angle, oleophobic angle, chemical structure, and flowability, respectively. We investigated the fire extinguishing effects of two extinguishing agents under different aging cycles, determined the endpoint of the lifespan, and predicted the storage life of ODPEA and SHOU DPEA at room temperature (25 °C).

Experimental and theoretical background

Thermal degradation theory

The fire-extinguishing agent particles within a sealed container tend to settle at the bottom due to the influence of gravity. Since the thermal decomposition reaction of sodium bicarbonate is non-reversible, pressurizing the gas does not affect the thermal decomposition rate of sodium bicarbonate. In this context, temperature becomes the primary accelerating factor for its aging. The relationship between temperature (T) and the rate constant (K(T)) of the chemical reaction is described by the Arrhenius equation[23], as expressed by Eq. (1):

$$K(T) = A \times \exp\left(-E_a/RT\right) \tag{1}$$

where *K(T)* represents the rate constant, *A* is a coefficient associated with ultrafine powder and the aging environment, E_a is the activation energy, *T* is the absolute temperature in Kelvin, and *R* is the universal gas constant (8.314 J/(mol*K)).

In the thermal aging process[24] of ODPEA and SHOU DPEA, the aging performance index A(t) is defined as the product of the rate constant K(t) and time (t), where t represents time. The time–temperature superposition approach[25] suggests that the aging performance obtained from short-term exposure at higher temperatures is equivalent to the aging performance obtained from long-term exposure at lower temperatures. Hence, Eq. (2) is derived.

$$K\left(T_1\right) \times t_1 = K\left(T_2\right) \times t_2 \tag{2}$$

Therefore, the aging time of SHOU DPEA at room temperature (25 °C) can be estimated as expressed in Eq. (3):

$$\frac{t_2}{t_1} = \frac{A \times \exp\left(-E_a/RT_1\right)}{A \times \exp\left(-E_a/RT_2\right)} \tag{3}$$

where t_1 and t_2 represent the times corresponding to temperatures T_1 and T_2, respectively.

Aging experiments

The preparation procedures and thermodynamic analyses of the ODPEA and SHOU DPEA used in this study have been thoroughly investigated in a separate article[15] and will not be repeated here. ODPEA and SHOU DPEA, as shown in Fig. 1, each weighing 1.2 kg, were individually placed into fire extinguisher bottles. Nitrogen gas was injected into the bottles to reach a pressure of 1.2 MPa. Subsequently, the fire extinguisher bottles were placed in an oven maintained at a constant temperature of 70 °C (considering the thermal decomposition characteristics of the extinguishing agent), and the pressure gauge readings were observed daily. If the pressure gauge on the fire extinguisher bottle exceeded 1.2 MPa, the gas would be released until the pressure returned to 1.2 MPa to prevent safety incidents caused by overpressure due to high temperatures. Every 40 days, 200 g of ODPEA and SHOU DPEA were collected following pressure release. The fire extinguisher bottles were resealed and pressurized to 1.2 MPa before being returned to the oven at a temperature of 70 °C. The experiment consisted of five cycles, each lasting 40 days. The experimental setup for the aging experiment is illustrated in Fig. 2.

Characterization

ODPEA and SHOU DPEA samples were observed for their microscopic morphology and particle size using a JSM-IT500HR scanning electron microscope (SEM) during each aging cycle. The particle size distribution of the samples was measured using a Mastersizer 3000 laser particle size analyzer from Malvern Instruments Ltd. The chemical structural changes in the samples were analyzed using a NICOLET IS10 Fourier-transform infrared spectrometer. The contact angles[26] of the samples with water and oil were measured using an SDC-100 Standard contact angle measurement instrument. 3 ml of deionized water and aviation kerosene were separately added into a standard syringe of 5 ml. 20 µl of liquid was dropped from the syringe at a distance of 1 cm from the powder surface, and the water contact angle and oil contact angle were calculated after allowing it to stand still.

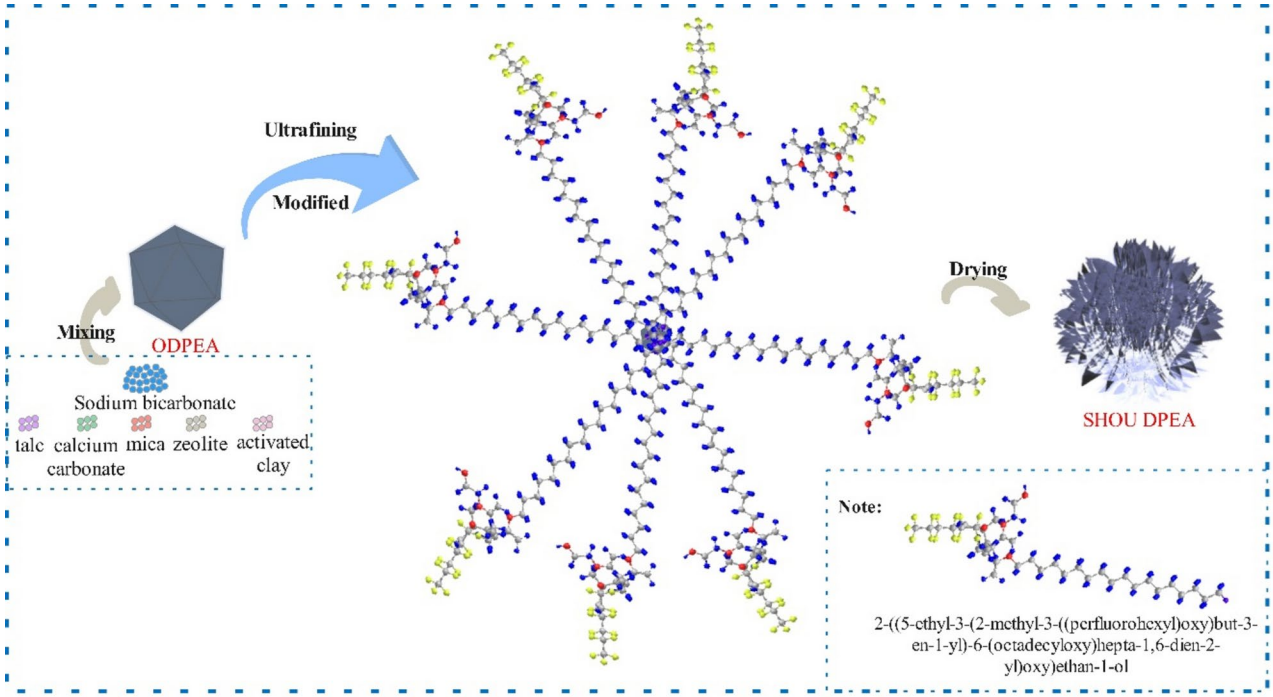

Fig. 1. Structure of ODPEA and SHOU DPEA.

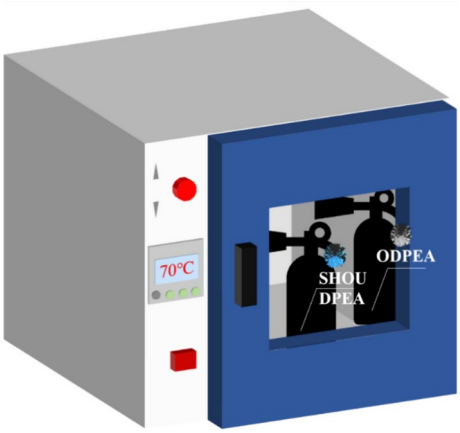

Fig. 2. Schematic diagram of the aging experiment (The software used is WPS (version 12.1.0.18912), with the official website link: [https://www.wps.cn/], and all elements are original works.)

To evaluate the flowability of the powder, we used the HY-100 A powder-tapped density meter to measure the powder's compacted bulk volume. The N/C ratio (vibration count divided by compression count) is the reciprocal of the vibration count (N), as described by Eq. (4)[27]. The reciprocal of the slope, denoted as l_p, is defined as the flowability index of the tested powder, while f_a represents the adhesion force of the powder particles as measured. Smaller values of l_p and f_a indicate better powder flowability.

$$\frac{N}{C} = \frac{1}{l_p} \cdot N + \frac{1}{l_p} \cdot f_a \tag{4}$$

A 0.1-cubic-meter fire extinguishing chamber was used to evaluate the effectiveness of the powder in extinguishing fires[27]. The chamber had a central region containing a circular steel oil pan with a diameter of 70 mm. Four thermocouples were positioned along the vertical axis above the oil pan, spaced at intervals of 0.08 m[28]. The environmental parameters are as follows: wind speed is 0.1 m/s, and humidity is 30%. The autonomously developed automatic ignition program is as follows: Upon triggering with a mouse click, temperature collection began, and automatic ignition followed after 1 s. After pre-burning for 119 s, concentration collection was initiated. After a 0.5-s delay, the high-speed cameras commence operation, followed by another 0.5-s delay before the electromagnetic valve was activated to release the pre-loaded powder from the powder storage tank. Each sample underwent three sets of fire extinguishing experiments, and any failure to extinguish the fire in any set was considered an overall failure. The maximum extinguishing concentration value among the three experiments was selected as the extinguishing concentration for that sample to avoid incidental errors.

Results and discussions

Microscopic morphology analysis

ODPEA

ODPEA exhibits distinct microsurface morphologies at various aging stages, as illustrated in Fig. 3. Before aging, ODPEA assumes an irregular triangular shape without pronounced edges, with all three sides measuring between 30 and 40 μm. The additives uniformly cover the surface of sodium bicarbonate, as depicted in Fig. 3a. On the 40th day (Fig. 3b), ODPEA exhibits a lamellar distribution with angular surfaces. Granular additives disperse near the substrate, with clear demarcation lines between particles. This phenomenon may arise from the gradual decomposition of sodium bicarbonate due to thermal effects, generating carbon dioxide. The fine particles on the surface are dispersed around the substrate due to the flow of carbon dioxide. Upon accelerated aging for 80 days (Fig. 3c), ODPEA transforms into a trapezoidal shape, and the substrate surface develops numerous tiny pores. The interfaces between the fine additive particles become blurred. While the particle shapes exhibit no significant changes compared to Fig. 3a, the edges of the particles gradually vanish, primarily due to water generation during the accelerated thermal decomposition, resulting in some adhesion in ODPEA. After 120 days of thermal aging, the trapezoidal ODPEA aggregates into a disc-like structure with crack formations, and a significant portion of the additives disperses in the vicinity, as shown in Fig. 3d. Following 160 days of aging (Fig. 3e), a significant transformation occurs in the surface morphology. Specifically, there are no apparent gaps between the ODPEA particles, giving rise to agglomeration. At the micrometer scale, a honeycomb-like pattern is observable on the surface of ODPEA, indicating a relatively loose aggregation of particles. The changes in microsurface morphology may suggest that the fire extinguishing agent could potentially become ineffective after prolonged aging. On the 200th day (Fig. 3f), ODPEA assumes a cauliflower-like structure at the micrometer scale, and the fine additive particles notably increase in size. This microsurface morphology of ODPEA is prone to block the nozzle of the fire extinguisher, making it difficult to spray out and reducing its flowability. Simultaneously, extensive caking results in a significant reduction in the extinguishing agent's surface area, leading to a decrease in its effectiveness against flames. The effectiveness of fire suppression may not be guaranteed.

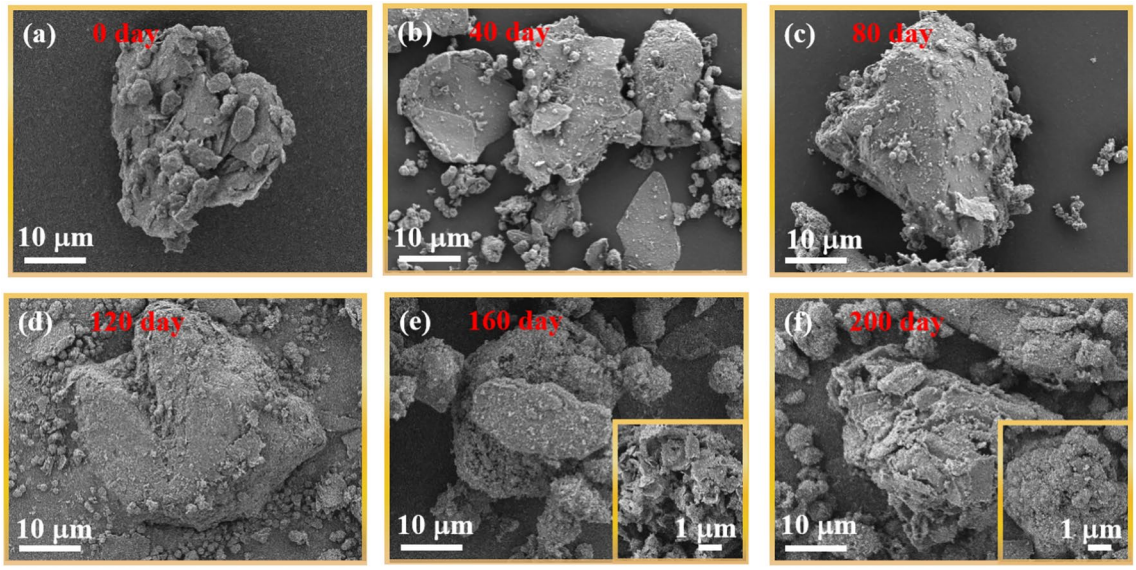

Fig. 3. Surface morphology of ODPEA at different aging cycles.

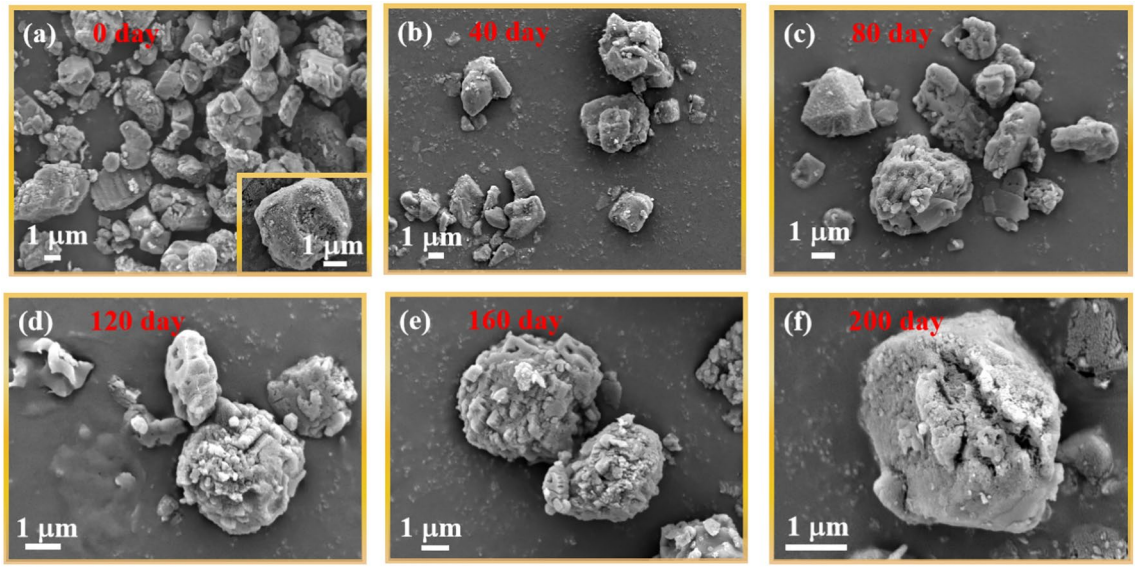

Fig. 4. Surface Morphology of SHOU DPEA at Different Aging Cycles.

SHOU DPEA

Figure 4 depicts the surface morphology of SHOU DPEA at various aging periods. The freshly prepared SHOU DPEA particles exhibit an average diameter of approximately 4–6 μm, with a particle surface coated by a fluffy hydrophobic and oleophobic layer, as illustrated in Fig. 4a. No significant changes in surface morphology are observed on the 40th day (Fig. 4b). The boundaries between particles remain distinct, and there is no apparent adhesion, indicating that the hydrophobic and oleophobic layers effectively prevent powder aggregation. Figure 4c reveals a slight blurring of boundaries between particles, indicating a potential decrease in the hydrophobic and oleophobic capabilities of SHOU DPEA with increased thermal aging time. On the 120th day (Fig. 4d), the particle size shows no significant increase, and the surface exhibits porous clustering, resulting in an increased surface area conducive to effective interaction with the fire source for rapid extinguishment. On the 160th day (Fig. 4e), small particles resembling the additives' size and shape appear on the SHOU DPEA's surface. As the aging duration increases, it implies that the hydrophobic and oleophobic layer undergoes damage, resulting in the exposure of underlying additive components that were previously encapsulated within the hydrophobic and oleophobic layers. Furthermore, on the 200th day, as depicted in Fig. 4f, two longitudinal cracks are visible on the particle surface. The cracked regions display numerous pores, while fewer pores are observed in the lower portions of the particles. During the 200-day accelerated aging process, there is minimal agglomeration

observed among SHOU DPEA particles, implying that the spray and flow resistance within the pipeline are relatively low. The specific surface area in contact with the flame does not significantly decrease, ensuring a better guarantee of the fire extinguishing effectiveness.

Comparison

Figure s1 (a) and (c) in the supplementary material represent the surface morphology of ODPEA and SHOU DPEA, respectively, before accelerated aging. ODPEAs exhibit large particle sizes with irregular surfaces. After undergoing hydrophobic and oleophobic modification and ultrafine treatment, the particle size of the fire extinguishing agents significantly decreases, and the particles assume a fluffy spherical shape. Following 200 days of accelerated thermal aging, ODPEA exhibits noticeable aggregation, forming cauliflower-like clustered structures on the surface, which further reduces the surface area. In contrast, SHOU DPEA particles largely maintain their independence, but cracks in the hydrophobic and oleophobic layer on the particle surface become evident. These cracks form numerous pores, while the lower sections remain relatively smooth without conspicuous cracking or pores. This observation is consistent with previous thermal analysis research findings[15], suggesting that the hydrophobic and oleophobic layer can shift the thermal decomposition temperature of SHOU DPEA, thereby extending its storage life.

D90 analysis

ODPEA

Figure 5 illustrates the particle size distribution of ODPEA at various aging periods. Detailed size distribution and cumulative distribution curves for each aging period are provided in the Fig. s2 in the supplementary material. Notably, the cumulative distribution curves shift towards large particle sizes as the aging periods increase, with a significant deviation observed at the 200-day case compared with other cases (0 to 160-day aging cases). To further analyze the particle size distribution, we focus on three key percentiles along the distribution curve: D10 (indicating 10% minimum particle size), D50 (reflecting the median of particle sizes), and D90 (indicating 90% particle size).

As shown in Fig. 5, the D10 of non-aged ODPEA is 0.72 μm, indicating that 10% of the particles have a size of 0.72 μm or less. As aging progresses to 40, 80, 120, and 160 days, the value of D10 increases to 1.25, 1.47, 1.54, and 1.67 times that of the initial value (0 aging cycle), respectively. However, on the 200th day of aging, the D10 value has reached 6.8 times that of the non-aged ODPEA. This implies that during the accelerated aging period of 160–200 days, the continuous high-temperature environment may lead to an increase in the surface energy of ODPEA, an increase in internal particle motion, easier contact between particles, and a significant occurrence of agglomeration and clumping, as observed in Fig. 3e and f. In comparison, the D50 value started to rapidly

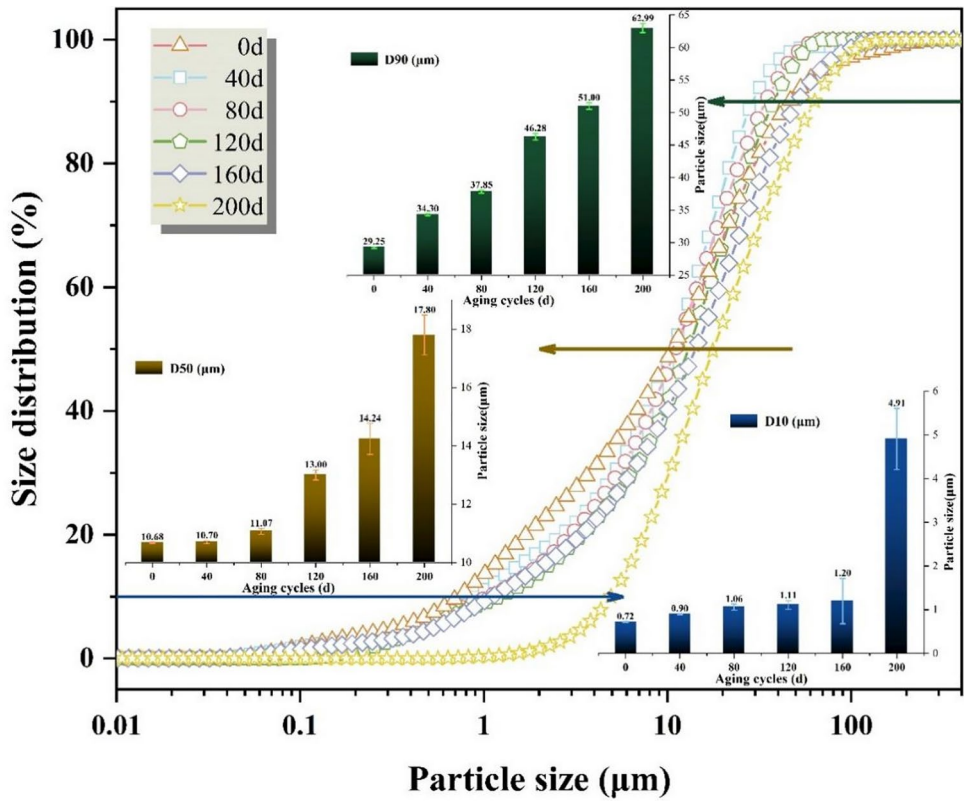

Fig. 5. Particle size distribution of ODPEA at different aging cycles.

increase after 120 days of aging, while the D90 exhibited linear growth from day 0 to 160, reaching 62.99 μm on the 200th day, exceeding the particle size requirements for dry powder extinguishing agents (D90: 20–60 μm)[29].

SHOU DPEA

Figure 6 depicts the particle size distribution of SHOU DPEA at various aging cycles, with detailed size distribution and cumulative distribution curves for each aging period available in Fig. s3 in the supplementary material. It can be observed that the particle size distribution curves of SHOU DPEA at aging periods of 0 days, 40 days, and 80 days almost overlap, indicating that during this period (0–80 days), SHOU DPEA undergoes minimal changes. On the 120th day, the values of D10, D50, and D90 are 3.5, 1.1 and 1.1 times that of those on the 80th day, suggesting an increased tendency for small particles to aggregate with prolonged thermal aging. This phenomenon may be attributed to the more pronounced Van der Waals forces between particles when the particle size is smaller, making smaller particles more prone to aggregation than larger ones. On the 160th day, the particle size distribution curve for SHOU DPEA resembles that of the 120th day. By the 200th day, the D10 value has increased to 5.7 times that of the initial value, and particles below 1μm have nearly disappeared, with 10% of particles falling in the range of 1.00–1.64 μm. Additionally, the D50 and D90 values have grown by 23% and 24%, respectively, compared to the initial values, with a relatively modest growth magnitude compared with the case of ODPEA. This could be attributed to the hydrophobic and oleophobic layer on the surface of SHOU DPEA, enhancing its thermal stability.

Comparison

Figure s4 in the supplementary material depicts the evolution of particle size for ODPEA and SHOU DPEA over the aging period. Notably, a significant inflection point is observed in the variation of particle size of ODPEA over time, occurring around 160 days. The growth in particle size of ODPEA can be divided into two distinct phases. The initial phase, which spans 0–160 days, is characterized by a gradual increase in the 90th percentile particle size length (L) over time (t) as the particles age. This relationship is well described by linear fits, with R^2 values of 0.984 for ODPEA, expressed as $L = 0.15t + 27.37$. During the following phase, which spans 160–200 days, ODPEA exhibits a significant increase in particle size, reaching 2.15 times initial states. Furthermore, The particle size growth against aging day of SHOU DPEA exhibits a single-stage, where the 90% particle length (L) shows a linear relationship with aging time (t), expressed as $L = 0.0062t + 5.18$, with R^2 values of 0.992. In comparison, the tendency of ODPEA to agglomerate is significantly higher than that of SHOU DPEA, resulting in reduced flowability and decreased fire suppression effectiveness.

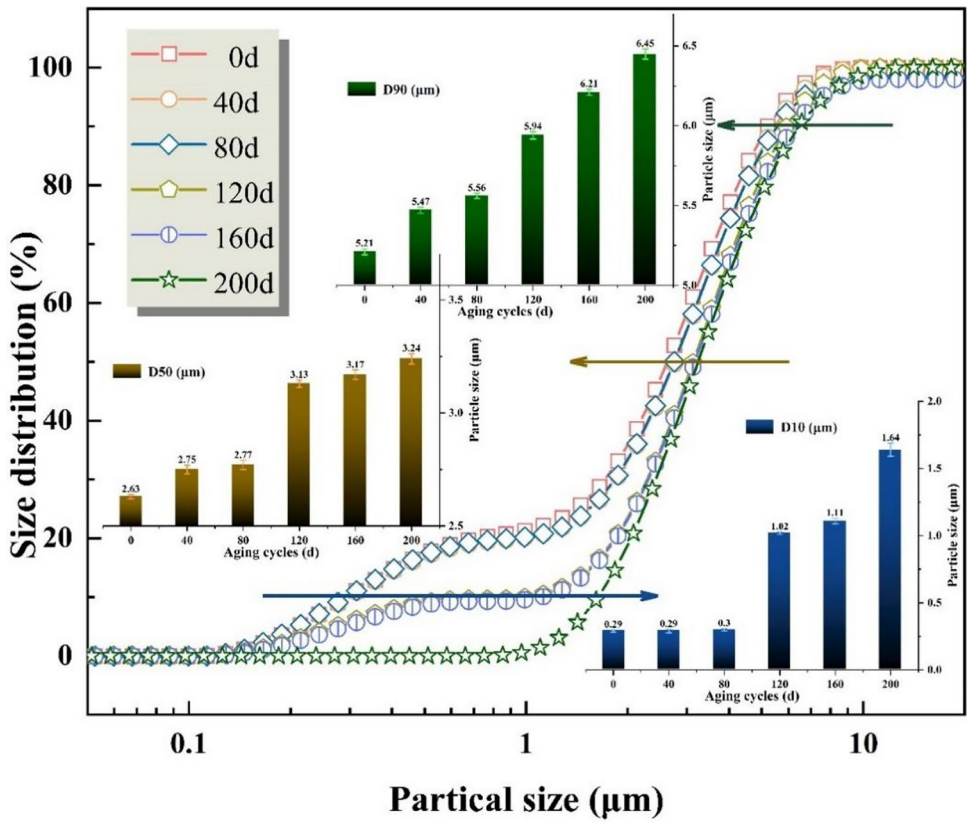

Fig. 6. Particle size distribution of SHOU DPEA at different aging cycles.

Infrared analysis

ODPEA

Figure 7 presents the infrared spectra of ODPEA at various aging periods. Prior to aging, the spectrum exhibits an absorption peak at 1700 cm^{-1}, attributed to the stretching vibration of the carboxyl functional group C=O in bicarbonate ions. The infrared absorption peaks at 1449.2 cm^{-1} and 826.8 cm^{-1} are attributed to the asymmetric stretching and bending vibrations of carbonate groups[30]. The infrared absorption peak at 990 cm^{-1} corresponds to the stretching vibration of the C-O group in NaHCO3. The peak at 3562 cm^{-1} corresponds to the bending vibration peak of the OH bond in water molecules, implying the potential presence of crystalline water in ODPEA[15].

On the 40th day and the 80th day of accelerated aging, a new absorption peak appears at 1394 cm^{-1}, possibly indicating the slow decomposition of sodium bicarbonate. Despite the continued bending vibration peak of the O–H bond, its intensity decreases compared to that at 0 day. As the accelerated aging time increases, the crystalline water content in ODPEA decreases, and the asymmetric stretching vibration peak of the carbonate group shifts. Additionally, an infrared absorption peak is detected at 871.2 cm^{-1}, which may be attributed to the asymmetric stretching vibration of the Si–O bond, a characteristic feature presenting in the additives of ODPEA, such as talc, mica, zeolite, and activated clay[31]. As observed in Fig. 3a and b, the ODPEA additives detach with aging.

After 120 days of aging, the infrared absorption peak at approximately 3562 cm^{-1} disappears, indicating the complete evaporation of crystalline water in ODPEA. At this point, the absorption peak at 1449 cm^{-1} disappears, while the peak around 1394 cm^{-1} remains constant. The variation in the infrared absorption peaks is primarily due to the impact of crystalline water on the asymmetric stretching vibration peak of the carbonate group, leading to a shift of the infrared peak towards higher wavenumbers. As aging progresses, the evaporation of crystalline water approaches completion, and the infrared peak returns to its original position. This indicates that untreated ODPEA possesses a relatively high moisture content. Under prolonged exposure to a thermal environment, the gradual evaporation of crystalline water leads to increased cohesion between the particles of ODPEA powder. This increased attraction makes agglomeration more likely, posing a challenge to its long-term sustainability.

During the aging process from 160 to 200 days, there are no significant changes in the position of the infrared absorption peaks. This could be attributed to the insignificant thermal decomposition of sodium bicarbonate or the overlap of the infrared spectra of sodium bicarbonate and sodium carbonate, which makes differentiation difficult.

SHOU DPEA

Figure 8 illustrates the infrared spectra of SHOU DPEA at different aging periods. Before aging, the spectrum exhibits an absorption peak at 1652 cm^{-1}, arising from the stretching vibration of the carboxyl functional group C=O in bicarbonate ions. In addition, the infrared absorption peaks at 1442 cm^{-1}, 1395 cm^{-1}, and 827 cm^{-1} are attributed to the asymmetric, symmetric, and bending vibrations of carbonate groups. The infrared absorption peak at 1075 cm^{-1} corresponds to the stretching vibration of the C–O group in $NaHCO_3$. Particularly, the infrared absorption peaks at 3223 cm^{-1} and 2860 cm^{-1} correspond to the stretching vibrations of hydroxyl groups (–OH) in FP and the stretching vibrations of C–H bonds in aliphatic hydrocarbons, respectively.

After 40 days of aging, there is no significant absorption peak in the 2800 cm^{-1}–3300 cm^{-1} spectral range, but a new infrared absorption peak is observed at 1917 cm^{-1}. This may result from the detachment of hydroxyl groups in the FP material during aging. The infrared absorption peak at 1910 cm^{-1} corresponds to the R–C(=O)–OR structure in the FP material. Notably, during the aging period from 40 to 80 days, the infrared absorption

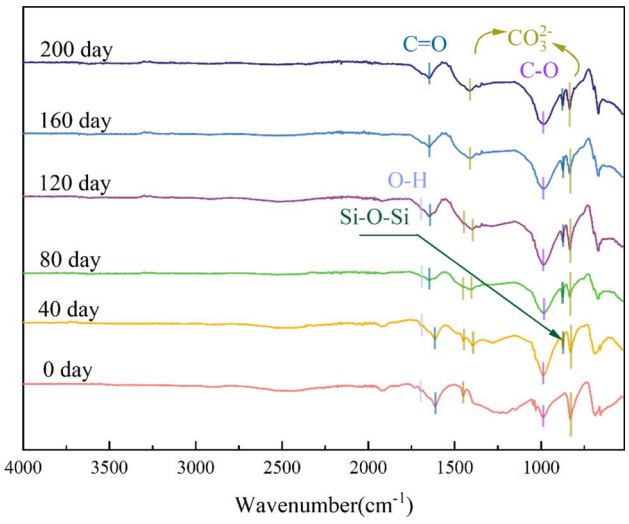

Fig. 7. Infrared spectra of ODPEA at different aging cycles.

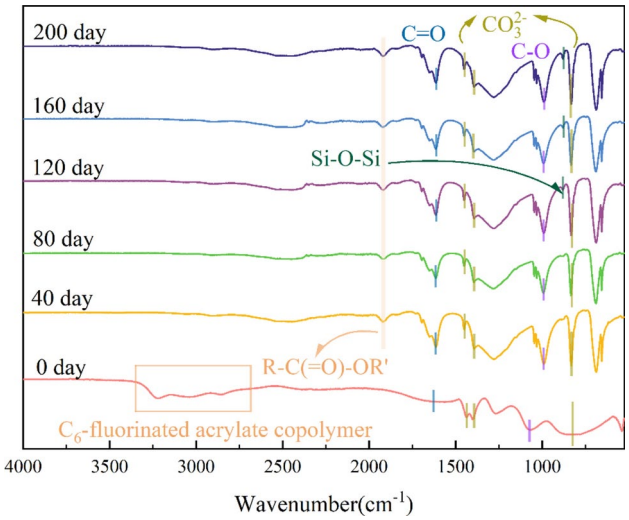

Fig. 8. Infrared spectra of SHOU DPEA at different aging cycles.

spectrum of SHOU DPEA remains constant, suggesting that SHOU DPEA may not undergo significant decomposition during this phase.

At 120 days of aging, an infrared spectrum peak corresponding to the Si–O bond is detected at 878 cm^{-1}[32,33]. This implies potential damage to the double hydrophobic layers, leading to the exposure of encapsulated additives. With increasing aging time, the intensity of the asymmetric stretching vibration peak of the Si–O bond increases, indicating a potential decrease in the hydrophobicity of SHOU DPEA over time.

Comparison

Figure s5 (a) in the supplementary material presents a comparative infrared spectroscopic analysis between untreated ODPEA and hydrophobic-hydrophobic modified SHOU DPEA before aging. The figure shows that untreated ODPEA contains –OH bonds, indicating the presence of crystalline water in its untreated state. In contrast, SHOU DPEA, after hydrophobic-hydrophobic modification with FP material, exhibits a coated surface, resulting in a more rounded shape for the infrared absorption peaks corresponding to the C=O, C–O, and bonds of sodium bicarbonate.

As depicted in Fig. s5 (b) in the supplementary material, nearly all crystalline water has evaporated from ODPEA, as evidenced by detecting an infrared spectrum peak corresponding to the Si–O–Si bond. Conversely, the Si–O–Si bond's infrared spectrum peak intensity in SHOU DPEA is comparatively lower. This suggests that, with increasing aging time, the hydrophobic- oleophobic layer on the surface of SHOU DPEA experiences a certain degree of damage, decreasing its storage lifespan.

XRD analysis

ODPEA

The XRD spectra of ODPEA at different aging cycles are shown in Fig. 9. Prior to aging, diffraction peaks corresponding to sodium bicarbonate (PDF#15-0700) are observed at 2θ values of 15.03°, 25.62°, 29.25°, 30.46°, 34.54°, 39.08°, 40.79°, 44.58°, 46.14°, and 47.75°. As shown in Fig. 9, both the positions and intensities of the diffraction peaks remain constant from 0 to 200 days of aging, suggesting that no significant structural changes occur in ODPEA during this period. However, after 160 days of aging, the diffraction peak at 25.62° significantly weakens, while those at 15.03° and 29.25° nearly disappear. This indicates that prolonged exposure to high temperatures leads to the decomposition or phase transformation of sodium bicarbonate, producing sodium carbonate, water, and carbon dioxide. Such a transformation disrupts the original crystal structure of sodium bicarbonate, resulting in the disappearance of its characteristic diffraction peaks. At 200 days of aging, the diffraction region between 25° and 35° exhibits a broad, diffuse peak instead of sharp diffraction peaks, and the intensities of the characteristic peaks of sodium bicarbonate (29.25° and 34.54°) are significantly reduced or completely vanish. This suggests that the crystal structure of sodium bicarbonate has been altered, potentially transforming into an amorphous phase or leading to particle agglomeration. These changes would reduce the material's crystallinity and, consequently, its detectability. Figure 3f provides further support for this observation.

SHOU DPEA

The XRD diffraction patterns of SHOU DPEA at different aging intervals are shown in Fig. 10. Before aging, diffraction peaks at 2θ angles of 14.12°, 24.76°, 28.19°, 29.35°, 33.73°, 38.42°, 40.09°, 43.82°, 45.33°, and 47.04° can be attributed to sodium bicarbonate (PDF#15-0700). Notably, a significant diffraction peak appears at 18°, corresponding to the characteristic peak of $C–F_2$ in the surface modifier FP material[34]. From Fig. 10, it can be observed that during 120 days of aging, the positions and intensities of the diffraction peaks for ODPEA remain almost constant, indicating that SHOU DPEA may not have undergone significant structural changes. At 160 days of aging, the intensity of the $C–F_2$ peak decreases with the increasing aging time, the diffraction peak

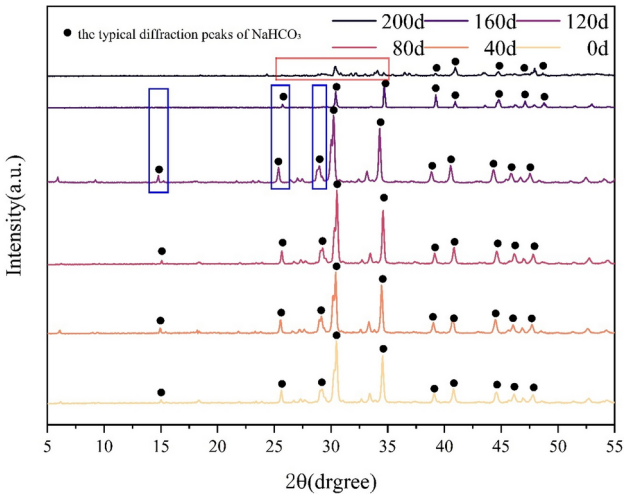

Fig. 9. XRD diffractogram of ODPEA at different aging cycles.

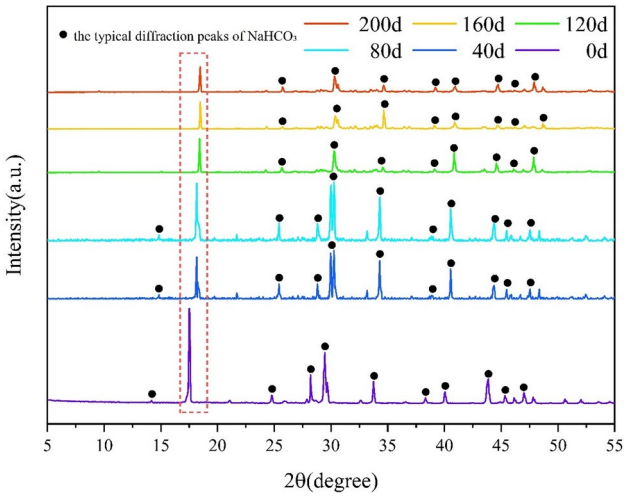

Fig. 10. XRD diffractogram of SHOU DPEA at different aging cycles.

at 14.12° disappears, and the intensity of the characteristic diffraction peaks for sodium bicarbonate at other positions also decreases to some extent with prolonged aging. However, the peak shapes do not show significant changes, suggesting that after 200 days of aging, the crystal structure of SHOU DPEA remains largely intact.

Comparison

Figure s6(a) in the supplementary materials presents a comparative analysis of the XRD diffraction patterns between untreated ODPEA and hydrophobic-hydrophobic modified SHOU DPEA before aging. Compared to ODPEA, the diffraction peaks of sodium bicarbonate in SHOU DPEA shift by approximately 1° towards lower 2θ angles. This shift is attributed to the strong hydrophobic groups and polar head groups of FP, which can form an ordered adsorption layer on the surface of the sodium bicarbonate crystals. This results in a slight increase in the interlayer spacing, causing the diffraction peaks to shift slightly. Furthermore, compared to ODPEA, SHOU DPEA exhibits stronger diffraction peak intensities, which may be due to the excellent hydrophobicity and chemical stability of the FP material. These properties help protect the surface of the sodium bicarbonate crystals, reducing damage caused by moisture and other environmental factors. This effect is more pronounced in Fig. s6(b), where at 200 days of aging, ODPEA shows some degree of decrystallization, and the crystal structure partially transitions to an amorphous state. In contrast, the sodium bicarbonate crystals in SHOU DPEA, which is coated with FP, maintain a more intact crystalline structure. This suggests that SHOU DPEA offers superior long-term storage performance compared to ODPEA.

Analysis of hydrophobic and oleophobic angles

The experiments demonstrate that when water or oil droplets come into contact with the surface of ODPEA, they rapidly immerse and disappear. The surface of ODPEA is thoroughly wetted by water (Fig. 11a), and due

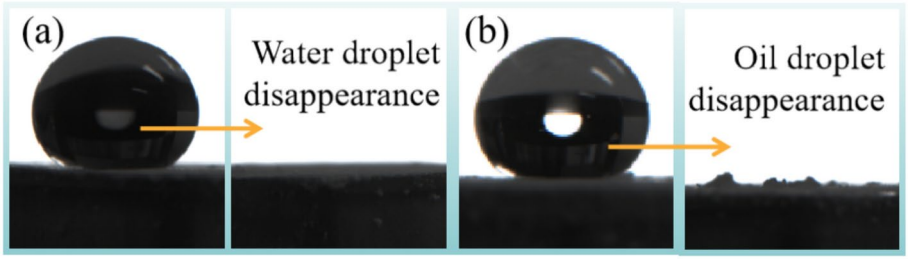

Fig. 11. Hydrophilic and oleophilic phenomena of ODPEA.

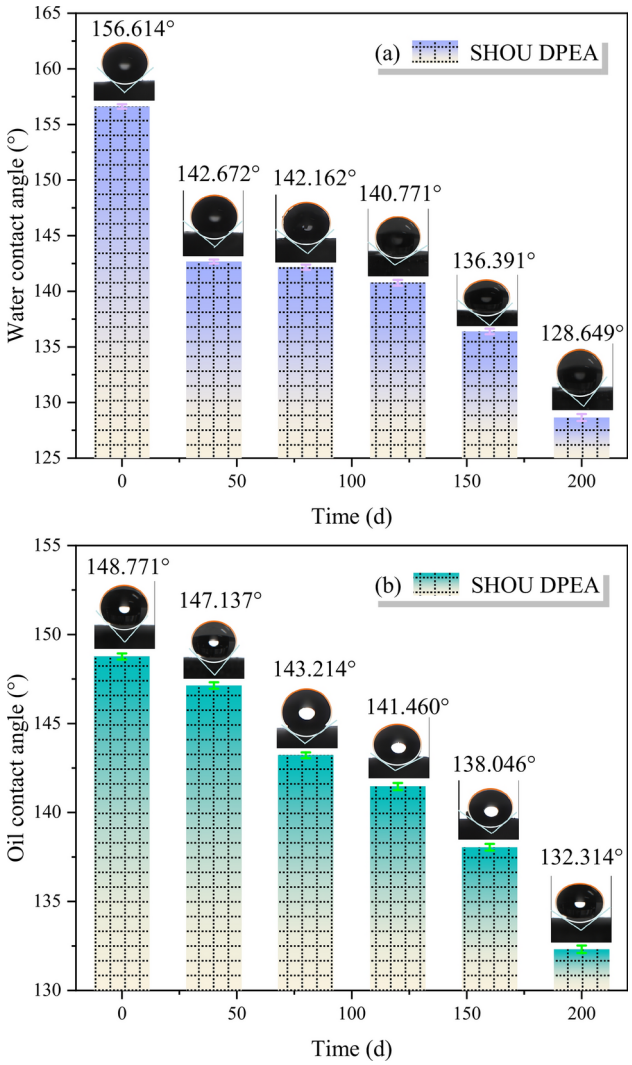

Fig. 12. Variation of contact angles of SHOU DPEA with aging time: (**a**) Hydrophobic angle, (**b**) Oleophobic angle.

to surface tension, a slight residue of oil droplets may remain on the ODPEA surface (Fig. 11b). Therefore, ODPEA lacks hydrophobic and oleophobic properties, indicating its hydrophilic and oleophilic behavior, which is unfavorable for storage and cleaning purposes.

The changes in water and oil contact angles of SHOU DPEA over time are illustrated in Fig. 12a and b, respectively. Before aging, SHOU DPEA exhibits a water contact angle of 156.614°, which exceeds 150°, showcasing its superhydrophobic characteristics. The oil contact angle is 148.771°, slightly below 150° but significantly exceeding 90°, indicating excellent oleophobic properties. On the 40th day, the water contact angle decreased to 142.672°, indicating the loss of superhydrophobic characteristics. The oil contact angle remains

relatively constant between 80 and 120 days of aging. On the 160th day, the water contact angle decreases to 136.391°. On the 200th day, the water contact angle decreases by 17.86% compared to its initial state. While the hydrophobic performance experiences a significant decline, it still exceeds 90°, meeting the requirements for hydrophobicity. The oil contact angle of SHOU DPEA decreases with increasing aging time, reaching 132.314° on the 200th day, representing an 11.06% decrease from the initial state. Notably, the initially higher water contact angle indicates greater superhydrophobicity compared to the oil contact angle. However, with accelerated aging, the rate of change in the oil contact angle is lower than that in the water contact angle. On the 200th day, the oil contact angle of SHOU DPEA exceeds the water contact angle. This suggests that the oleophobic properties of SHOU DPEA are less affected by heat. After firefighting in aircraft engines, SHOU DPEA is less likely to dissolve in oil, making cleaning less challenging.

Flowability analysis

ODPEA

To investigate the changes in the flowability performance of ODPEA over aging time, we measured the compressibility (N/C) data of ODPEA at different vibration frequencies (N). The compressibility versus the number of vibrations for ODPEA at different aging times is shown in Fig. 13. Samples sp-1 to sp-6 conform to linear equations $N/C = 3.94N + 62.06$, $N/C = 4.72N + 98.02$, $N/C = 3.60N + 81.25$, $N/C = 4.43N + 110.30$, $N/C = 4.12N + 123.35$, and $N/C = 4.03N + 251.56$, respectively, with R^2 all exceeding 0.986 (refer to supplementary material Tab.s1 for detailed data).

According to Eq. (4), the flowability index (I_p) of ODPEA is found to be 0.25, 0.21, 0.28, 0.23, 0.24, and 0.25 for samples sp-1 to sp-6, respectively. The maximum flow index is 12% higher than that before aging. The interparticle adhesion force (f_a) of ODPEA is measured as 15.74, 20.76, 22.57, 24.90, 29.91, and 62.40 for samples sp-1 to sp-6, respectively. From 0 to 120 days, the f_a of ODPEA gradually increases with aging time. On the 160th and 200th days, the f_a rapidly increases, rising by 90% and 296.44%, respectively, compared to the non-aged ODPEA. Interestingly, a similar phenomenon was also observed in the trend of ODPEA particle size over time, as depicted in Fig. s4 in the supplementary material. It can be inferred that the particle size changes in ODPEA are positively correlated with its flowability. With an increase in aging time, the adhesion force (f_a) rapidly increases, leading to higher internal friction between particles and decreased flowability.

SHOU DPEA

The compressibility data (N/C) for SHOU DPEA at different vibration frequencies (N) can be found in Supplementary Material Tab.s2. The compressibility versus the number of vibrations for SHOU DPEA at different aging times is depicted in Fig. 14. Samples sp-1 to sp-6 exhibit linear equations $N/C = 3.31N + 146.76$, $N/C = 3.31N + 181.20$, $N/C = 2.68N + 175.64$, $N/C = 3.12N + 216.00$, $N/C = 2.70N + 228.43$, and $N/C = 3.04N + 273.34$, respectively, with R^2 all exceeding 0.995.

According to Eq. (4), the flowability index (I_p) of SHOU DPEA is found to be 0.30, 0.30, 0.37, 0.32, 0.37, and 0.33 for samples sp-1 to sp-6, respectively. The maximum flow index is 23% higher than that before aging. The interparticle adhesion force (f_a) of SHOU DPEA is measured as 44.27, 54.72, 65.57, 69.23, 70.04, and 75.61, respectively. The interparticle adhesion force of SHOU DPEA increases with aging over time. The adhesion force in the 2nd, 3rd, 4th, 5th and 6th cycles increase by 23.60%, 48.11%, 56.38%, 58.21%, and 70.80%, respectively, compared to those on the 1st cycle.

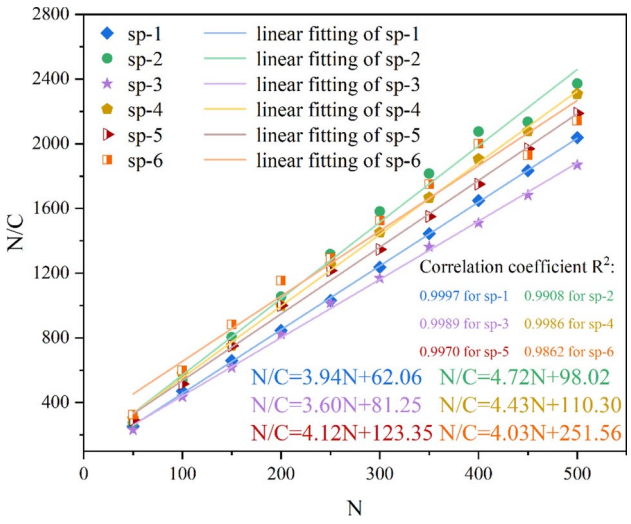

Fig. 13. Relationship between compressibility and vibration frequency of ODPEA at different aging cycles. (Where, sp-1, sp-2, sp-3, sp-4, sp-5, sp-6 correspond to samples aged for 0 days, 40 days, 80 days, 120 days, 160 days, and 200 days, respectively.)

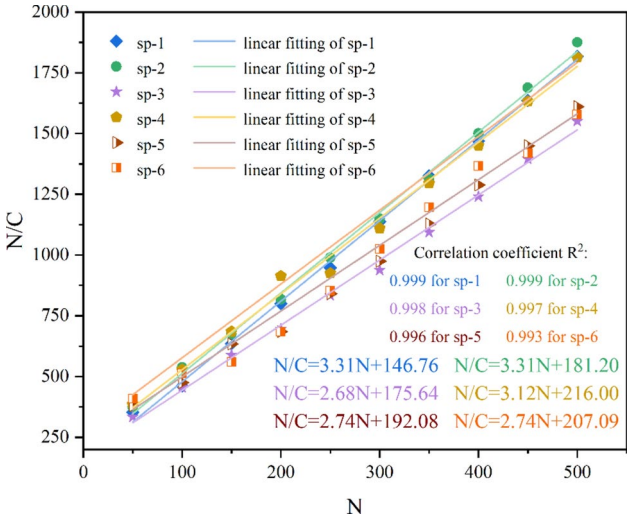

Fig. 14. Relationship between compressibility and vibration frequency of SHOU DPEA at different aging cycles. (Where, sp-1, sp-2, sp-3, sp-4, sp-5, sp-6 correspond to samples aged for 0 days, 40 days, 80 days, 120 days, 160 days, and 200 days, respectively.)

Comparison

Figure s7 in the supplementary material presents a comparison of the interparticle adhesion force (f_a) between ODPEA and SHOU DPEA. The interparticle adhesion force of SHOU DPEA is significantly higher than that of ODPEA, indicating that the flowability of SHOU DPEA is inferior to that of ODPEA. This is primarily attributed to the significantly smaller particle size of SHOU DPEA compared to ODPEA. As the powder particle size decreases, the molecular and electrostatic forces between particles increase, making the particles more prone to adhesion. This increased interparticle adhesion leads to higher internal friction, resulting in denser particle packing, reduced permeability, increased compressibility, and decreased flowability. Additionally, the f_a values of both ODPEA and SHOU DPEA increase with aging time. On the 200th day, the f_a value of SHOU DPEA is 1.71 times that of the non-aged SHOU DPEA, while the f_a value of ODPEA on the 120th day is 1.58 times that of the non-aged ODPEA. On the 160th and 200th days, the f_a values reach 1.90 times and 3.97 times of the non-aged SHOU DPEA, respectively. The increase in f_a is much higher than that of SHOU DPEA at the same time, indicating that ODPEA experiences a rapid growth in adhesion strength and reduced liquidity after 160 days of aging.

The analysis of fire extinguishing efficiency

ODPEA

In order to investigate the changes in the fire-extinguishing efficiency of ODPEA after prolonged storage, fire-extinguishing experiments on a typical oil pool fire (aviation kerosene fire (RP-3)) were performed. A control program was developed to ensure the consistency of ignition, pre-burning, and spraying timing of the fire extinguishing agent. High-speed photography was used to capture images, and a deep learning algorithm was used to extract flame morphology and height data during the process of extinguishing the fire. The fire was considered to be extinguished when the flame height reached zero in the next high-speed photo, determining the extinguishing time. Figure 15 depicts the flame morphology changes during the process of ODPEA extinguishing *n*-heptane fire at different aging periods, while Fig. s8 in the supplementary material illustrates the variation in flame height and extinguishing time throughout this process.

Figure 15a illustrates the fire extinguishing process of 0-day aged ODPEA. Visually, at the moment of ignition, the flame appeared relatively small. Following 120 s of adequate pre-burning, the flame became more stable and brighter. Upon spraying non-aged ODPEA for a duration of 0.100 s, ODPEA interacted with the flame, creating a hollow section in the middle of the flame. At 120.300 s, the flame appeared at waist level, and the body was segmented by ODPEA, resulting in an unusually bright flame. Subsequently, the flame gathered again, and at 121.028 s, the flame height significantly decreased, undergoing multiple changes in flame morphology, ultimately being extinguished completely.

For the 40-day aged ODPEA (Fig. 15b), when exposed to the flame for 0.400 s, the flame section was being segmented. After 120.600 s, the flame became bright, resembling scattered fireworks. After 120.800 s, the flame gathered again and enlarged, at which point the flame turned dark red. Subsequently, the flame was fragmented until it was extinguished at 121.198 s.

In Fig. 15c and Fig. s8 in the supplementary material, it can be observed that for the 80-day-aged ODPEA, the flame was cut off when the aged ODPEA interacted with the flame for 0.200 s. From 120.200 to 120.600 s, the flame flickered intermittently, resembling a chain, but at 120.800 s, the flame was recombined and took on a deep red color. At 121.000 s, the flame took on a circular shape with visible bright spots. After 121.200 s, the flame became smaller and darker, with a rapid decrease in flame height. However, at 121.400 s, the flame increased in size again. This indicates that the extinguishing effectiveness of the ODPEA was further reduced and the flame

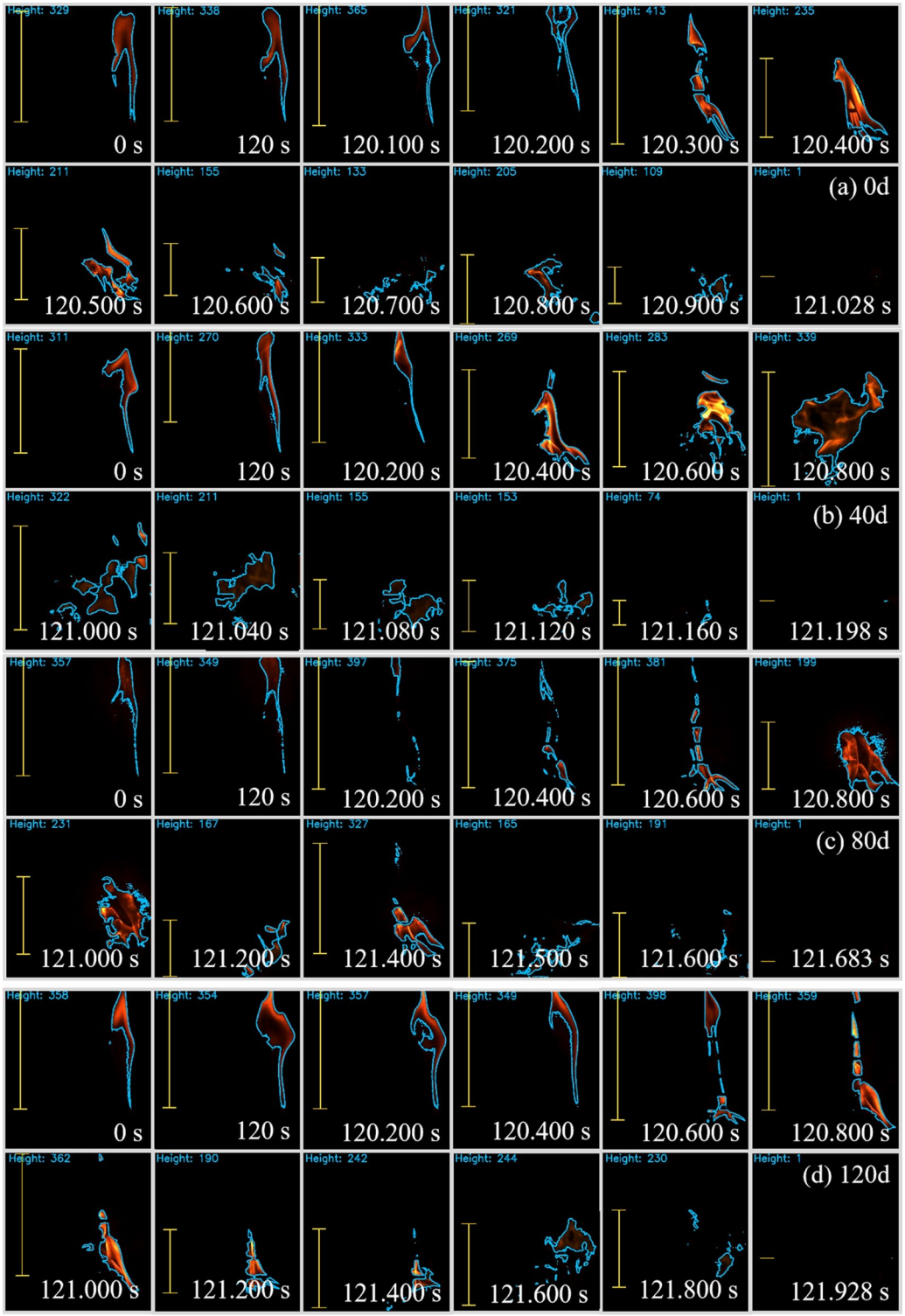

Fig. 15. Morphological changes of *n*-heptane fire extinguished by ODPEA at different aging cycles.

fluctuated in size during the extinguishing process, engaging in a repetitive tug-of-war, and the extinguishing time was 1.683 s.

The changes in flame morphology for the cases of the 120-day-aged and 160-day-aged ODPEA were similar to those for the case of 80-day-aged ODPEA. In these two cases, as shown in Fig. s8, when ODPEA interacted with *n*-heptane flames, the flame oscillated repeatedly, and the extinguishing time were 1.928 s and 3.121 s, respectively. However, after aging for 200 days, ODPEA failed to extinguish the *n*-heptane flame even after 125.000 s.

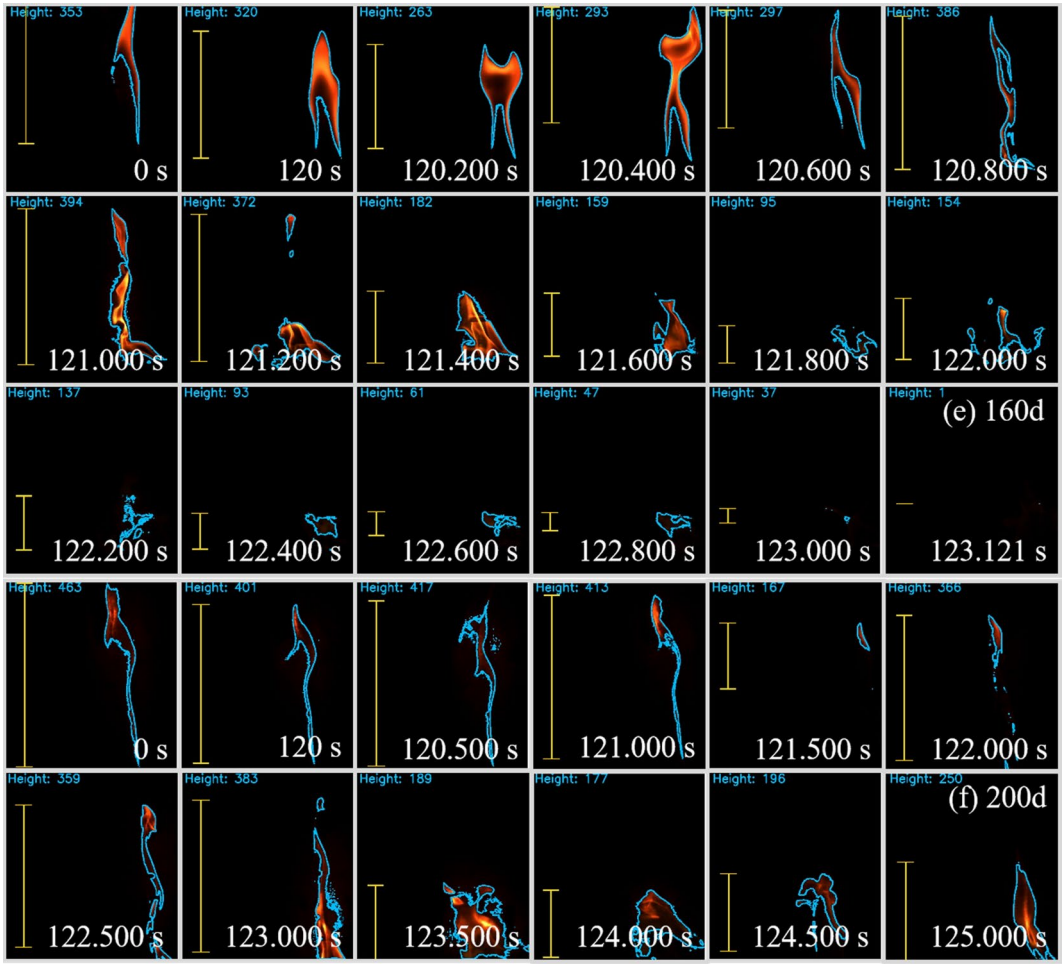

Figure 15. (continued)

SHOU DPEA

Figure 16 and Fig. s9 in the supplementary material depict the flame morphology, flame height, and extinguishing time of SHOU DPEA in extinguishing *n*-heptane fires at the cases of different aging periods. After SHOU DPEAs were sprayed, it rapidly interacted with the *n*-heptane flame, extinguishing it in only 0.094 s. The fire extinguishing times for SHOU DPEA with aged 40, 80 and 120 days against *n*-heptane fires were 0.097s, 0.12s, and 0.164s respectively (Fig. s9). For the case of 160 aging days, as shown in Fig. 16e, the center of flame was hollow at 120.04 s, resembling that the flame swallowed SHOU DPEA, followed by the oscillations at the base of the flame. The flame gradually turned into fragments for 0.2s, but at 120.24 s, it expanded again and then slowly diminished with the extinguishing time of 0.264 s. From Fig. 16f and Fig. s9, it can be observed that the base of the flame continues to oscillate for a few milliseconds. During the interaction between SHOU DPEA and the flame, the flame remains bright yellow, and the extinguishing time increases to 0.283 s.

Comparison

The effectiveness of fire extinguishing is a critical measure for evaluating the performance of fire extinguishing agents. We obtain the initial light intensity (I_0) through laser excitation. Subsequently, we inject ODPEA or SHOU DPEA at various known concentrations and document the laser light intensity (I) after achieving a uniform distribution of ODPEA or SHOU DPEA in space, which satisfies Eqs. (5) and (6), respectively.

$$-\ln I/I_0 = 0.0037C_e \tag{5}$$

$$-\ln I/I_0 = 0.01474C_e \tag{6}$$

where I_0 and I represent the initial light intensity and the light intensity after the fire extinguishing agent concentration reaches a constant value, and C_e is the concentration of the fire extinguishing agent.

Figure 17 compares the extinguishing time and concentration between ODPEA and SHOU DPEA at different aging periods. For the 0-day-aged ODPEA, the fire extinguishing concentration and time were 88.03 g/m^3 and 1.028 s, respectively (Fig. 17a). Furthermore, for the 160-day-aged ODPEA, the extinguishing concentration reaches 97.37 g/m^3, which is more than 10% higher than the extinguishing concentration of the 0-day-aged

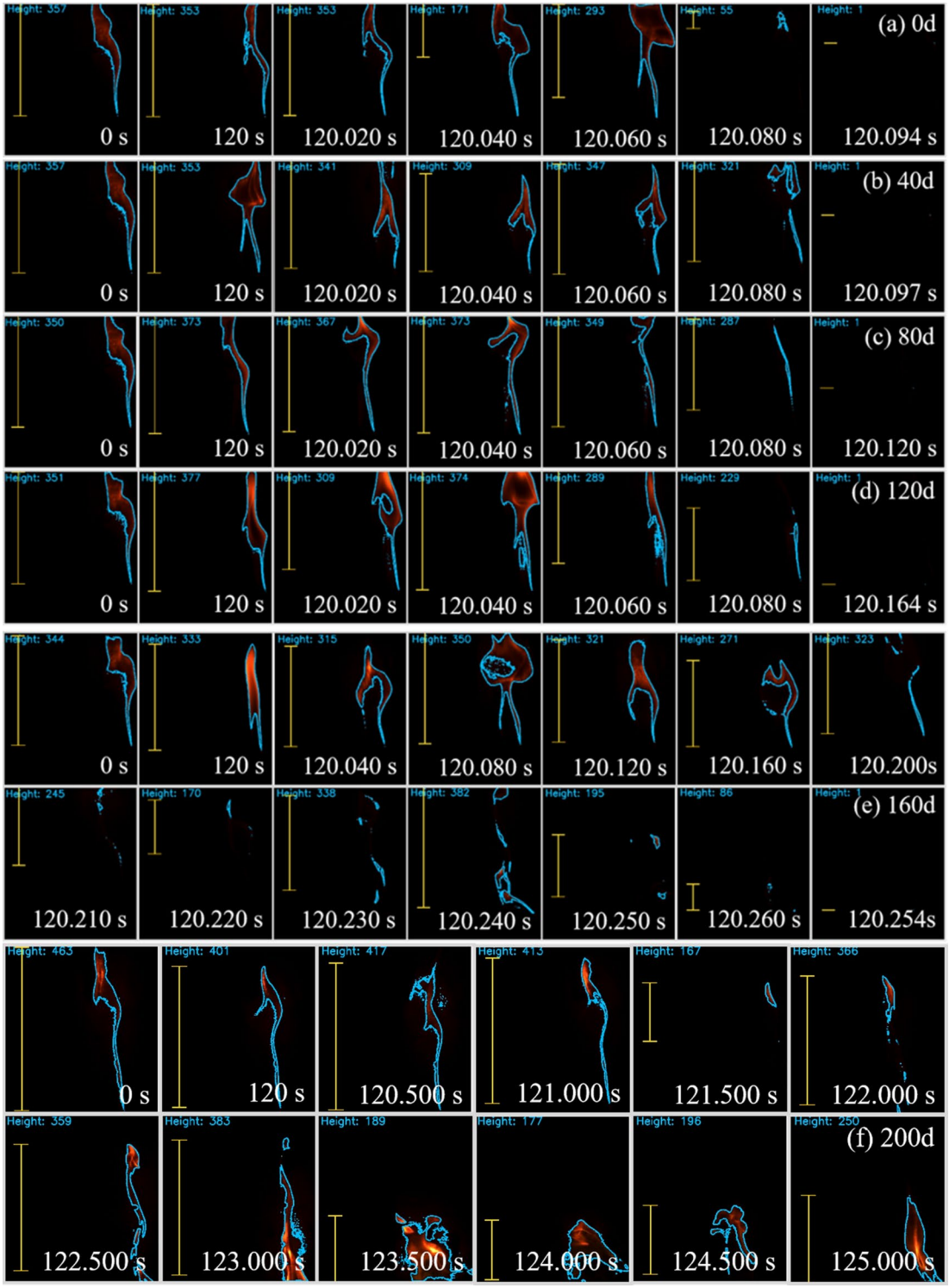

Fig. 16. Morphological changes of *n*-heptane flame extinguished by SHOU DPEA at different aging cycles.

ODPEA, and the extinguishing time is more than 3 times that of the 0-day-aged ODPEA. Even on the 200th day, ODPEA can no longer extinguish the *n*-heptane pool fire. Therefore, prolonged exposure to heat for 160 days or more will significantly reduce the fire-extinguishing effectiveness of ODPEA.

For SHOU DPEA with 0 days of aging, the extinguishing concentration is 31.70 g/m3, and the extinguishing time is 0.094 s. From Fig. 17b, it can be observed that during the aging process, even though the extinguishing time and extinguishing concentration of SHOU DPEA both increase, but the increase in extinguishing concentration is less than 10%. In particular, on the 200th day, the extinguishing time of SHOU DPEA is 0.283 s, only 27.5%

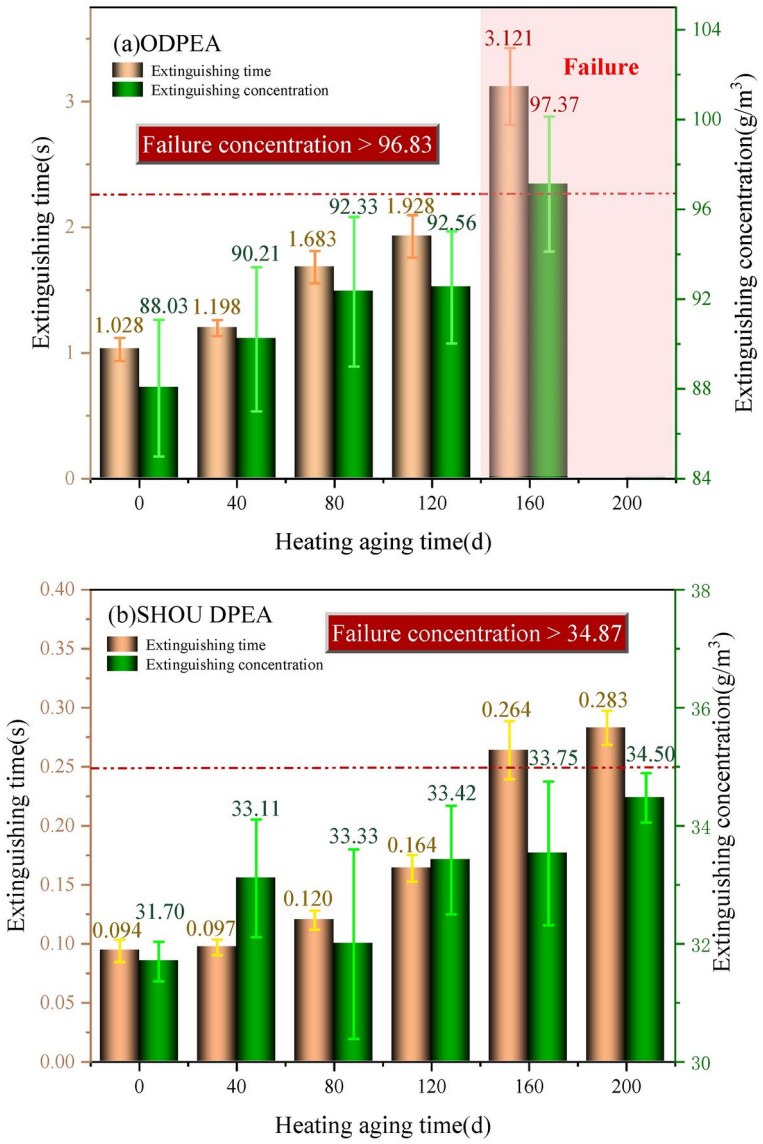

Fig. 17. Comparison of extinguishing time and extinguishing concentration between ODPEA and SHOU DPEA.

of the extinguishing time of ODPEA with 0 days of aging. This implies that SHOU DPEA can maintain its fire-extinguishing effectiveness at a relatively ideal level even after undergoing 200 days of accelerated heat aging.

Service life

Powder-based fire extinguishing agents differ from gas-based agents due to the heterogeneous stability of each component. Therefore, lifespan of powder-based fire extinguishing agents is influenced by many factors: (1) Particle Size Increase during Long-term Storage: Extended storage can lead to an increase in particle size, which may reduce flowability. In severe cases, this can result in the inability to spray or insufficient discharge, rendering the extinguishing agent ineffective. (2) Hydrophilicity and Aggregation: The hydrophobic nature of fire extinguishing agents is advantageous in preventing aggregation. Agglomerated extinguishing agent particles have a reduced surface area, leading to decreased contact with the flame during firefighting. This phenomenon may render the extinguishing agent ineffective. (3) Slow Decomposition of Extinguishing Agents: The gradual breakdown of extinguishing agents reduces the content of effective fire-extinguishing components, resulting in a decrease in extinguishing efficiency. Therefore, the flow characteristics of the fire extinguishing agent within the pipeline, along with the active extinguishing components, collectively determine the efficiency and extinguishing time of the fire suppression.

Table 1 presents the performance parameters of ODPEA at different aging periods. It can be observed that the absorption peaks corresponding to crystalline water in the ODPEA infrared spectrum disappears between 160 and 200 days. The disappearance of crystalline water indicates an increased mutual attraction between powder particles and a greater likelihood of agglomeration. Interestingly, at the macro level, the flowability

Performance Parameters	0d	40d	80d	120d	160d	200d	Critical point
SEM	No apparent agglomeration				Clumping		Clumping
D90 (μm)	L=0.15t+27.37					62.99	⩽ 60
IR	O-H				Evaporation of crystalline water		H_2O
Hydrophobic angle (°)	Hydrophilic						⩾ 90
Oleophobic angles (°)	Hydrophobic						⩾ 90
Flowability	1	1.32	1.43	1.58	1.9	3.97	1.9
Extinguishing time (s)	1.028	1.198	1.683	1.928	3.121	Failure	-
Fire extinguishing concentration (g/m^3)	88.03	90.21	92.33	92.56	97.37	Failure	96.83
Predicted lifespan (day)	2715 (25 °C)						120 (70 °C)

Table 1. Performance parameters of ODPEA at different aging cycles.
Assuming the interparticle adhesion force (f_a) of non-aged ODPEA as 1 (dimensionless), calculate the f_a multiples on the 40th, 80th, 120th, 160th, and 200th day compared to non-aged ODPEA.

Performance Parameters	0d	40d	80d	120d	160d	200d	Critical point
SEM	No apparent agglomeration						Clumping
D90 (μm)	L=0.0062t+5.18						⩽ 20
IR	No crystalline water						H_2O
Hydrophobic angle (°)	156.614	142.672	142.161	140.771	136.391	128.649	⩾ 90
Oleophobic angles (°)	148.771	147.137	143.214	141.460	138.046	132.314	⩾ 90
Flowability	1	1.24	1.48	1.56	1.58	1.71	1.9
Extinguishing time (s)	0.094	0.097	0.120	0.164	0.254	0.283	-
Fire extinguishing concentration (g/m^3)	31.70	33.11	33.33	33.42	33.75	34.50	34.87
Predicted lifespan (day)	> 4525 (25 °C)						> 200 (70 °C)

Table 2. Performance parameters of SHOU DPEA at different aging cycles.
Assuming the interparticle adhesion force (f_a) of non-aged SHOU DPEA as 1 (dimensionless), calculate the f_a multiples on the 40th, 80th, 120th, 160th, and 200th day compared to non-aged SHOU DPEA.

indicator (interparticle adhesion force) and the fire extinguishing effectiveness indicator (fire extinguishing concentration) for the ODPEA aged for 160 days exceed 90% and 10%, respectively, compared to the untreated state. This indicates a significant decrease in the flowability and fire-extinguishing performance of ODPEA after 160 days of aging. According to the "barrier effect" principle and safety considerations, the accelerated aging failure time of ODPEA should be within the range of 120–160 days. Based on the thermal failure theory in Section "Aging experiments", the predicted storage lifespan at room temperature (25 °C) is 2715 days, exceeding the recommended 5-year lifespan for dry powder extinguishing agents for buildings. However, it fails to meet the 10-year lifespan requirement for aviation fire suppressants.

Table 2 illustrates performance parameters for SHOU DPEA at various aging periods. It is gratifying that during the 200-day accelerated aging process, SHOU DPEA meets all performance criteria. According to the thermal failure theory in Section "Aging experiments", the predicted storage lifespan at room temperature (25 °C) is 4525 days, exceeding the 10-year threshold[19]. This implies that SHOU DPEA may be effectively stored on aircraft.

Conclusions

In this paper, we investigated the influence of different aging cycles on various parameters of ODPEA and SHOU DPEA. The study focused on the evolution patterns of microscopic morphology, D90 distribution, infrared characteristics, hydrophobic and oleophobic properties, extinguishing time, and extinguishing effectiveness for both ODPEA and SHOU DPEA. The concentration at which failure occurs and the endpoint of lifespan were established through this research. The conclusions of this study are as follows:

(a) Compared with ODPEA, SHOU DPEA exhibits smaller particle size and more regular particle shape, which contributes to an increased storage lifespan.
(b) The D90 value of ODPEA with aging time exhibits two stages: a slow growth stage (0–160 days), the D90 values of ODPEA satisfy equation L = 0.14t + 28.64. During the second stage (160–200 days), there is a rapid

increase in particle size. Additionally, the D90 values of SHOU DPEA satisfy equation L = 0.0062t + 5.18 throughout the entire accelerated aging process.

(c) The infrared spectra and contact angle analysis of ODPEA and SHOU DPEA reveal that SHOU DPEA exhibits significantly superior heat stability and flowability compared to ODPEA.

(d) The flowability equations for ODPEA after aging for 0, 40, 80, 120, 160, and 200 days are N/C = 3.94N + 62.06, N/C = 4.72N + 98.02, N/C = 3.60N + 81.25, N/C = 4.43N+110.30, N/C = 4.12N + 123.35, and N/C = 4.03N + 251.56, respectively.

(e) For SHOU DPEA after aging for 0, 40, 80, 120, 160, and 200 days, the flowability equations are N/C = 3.31N + 146.76, N/C = 3.31N + 181.20, N/C = 2.68N + 175.64, N/C = 3.12N + 216.00, N/C = 2.70N + 228.43, and N/C = 3.04N + 273.34, respectively.

(f) The thermal failure aging time of ODPEA and SHOU DPEA is greater than 120 days and 200 days, respectively. The predicted storage life of ODPEA at room temperature (25 °C) is 2715 days, while the predicted storage life of SHOU DPEA at room temperature (25 °C) is greater than 4525 days.

Data availability

Data available on request from the authors. The data that support the findings of this study are available from the corresponding author upon reasonable request.

Received: 17 October 2024; Accepted: 21 January 2025
Published online: 29 January 2025

References

1. Li Si-cheng, B. S., Prediction and analysis of hydrofluorocarbons phase-out management China's fire-fighting industry. **41**, 698 (2022).
2. Pagliaro, J. L., Linteris, G. T., Sunderland, P. B. & Baker, P. T. Combustion inhibition and enhancement of premixed methane–air flames by halon replacements. *Combust. Flame* **162**, 41 (2015).
3. Wang, Y. W., Zou, G. W., Liu, C. L. & Gao, Y. Comparison of fire extinguishing performance of four halon substitutes and Halon 1301. *J Fire Sci.* **39**, 370 (2021).
4. Yang, X. The research on discharge performance of civil aircraft fine dry powder fire extinguishing system. *Civ. Aircr. Design Res.* **119**, 26 (2015).
5. Ma, W. T., Fu, Y. Y., Zhao, J. C., Lu, S. & Zhang, H. P. Ultra-fine powder extinguishing agent concentration measurement based on extinction method. *Opt. Eng.* **60**, 094110 (2021).
6. Du, D., Shen, X., Feng, L., Hua, M. & Pan, X. Efficiency characterization of fire extinguishing compound superfine powder containing Mg $(OH)_2$. *J. Loss Prev. Proc.* **57**, 73–80 (2019).
7. Min, H., Dayong, X., Ru, Z., Xuhai, P. & Renming, P. Simulation research of superfine powder extinguishing agent movement. *Proc. Eng.* **45**, 1031 (2012).
8. Guo, X. et al. Experimental and numerical simulation research on fire suppression efficiency of dry powder mediums containing molybdenum flame retardant additive. *Process. Saf. Environ.* **159**, 294 (2022).
9. Zhang, Y., Hou, H. R., Wang, Y. W., Pan, R. M. & Zhou, X. Preparation of NaHCO3 fire extinguishing agent with perfluoropolyether groups to inhibit rapid re-ignition of Class B fires. *Colloid Surf. A* **691**, 133881 (2024).
10. Wang, Z. X. et al. Study on the pyrolysis and fire extinguishing performance of high-temperature-resistant ultrafine dry powder fire extinguishing agents for aviation applications. *Molecules* **29**, 3500 (2024).
11 XiaogangGuo, T. L. A. J. In situ molecule-level interface tailoring of metastable intermolecular composite chips toward on-demand heat release and information encryption. *J Mater. Chem. A* **11**, 26465 (2023).
12. Zhao, J. et al. Superhydrophobic and oleophobic ultra-fine dry chemical agent with higher chemical activity and longer fire-protection. *J Hazard. Mater.* **380**, 120625 (2019).
13. Zhang, Y., Hou, H., Wang, Y., Pan, R. & Zhou, X. Preparation of NaHCO3 fire extinguishing agent with perfluoropolyether groups to inhibit rapid re-ignition of Class B fires. *Coll. Surf. A Physicochem. Eng. Asp.* **691**, 133881 (2024).
14. Ning, W., Yang, Y., Zhang, D. & Pan, R. Surface modification of sodium bicarbonate ultrafine powder extinguishing agent by environmental friendly fluorinated acrylate copolymers. *Polym. Degrad Stabil.* **187**, 109558 (2021).
15. Liu, Y. et al. Comparative study on pyrolysis characteristics, kinetics, volatile products and chemical reactions of novel superhydrophobic and oleophobic ultra-fine and ordinary dry powder extinguishing agent. *J. Anal. Appl. Pyrol.* **172**, 106034 (2023).
16. Gong, H. W. A. J. A comparative study of GA, PSO and SCE algorithms for estimating kinetics of biomass pyrolysis. *Emerg. Manag. Sci. Technol.* **3**, 9 (2023).
17. Zhao, G. M., Xu, G. J., Jin, S., Zhang, Q. S. & Liu, Z. X. Fire-extinguishing efficiency of superfine powders under different injection pressures. *Int. J. Chem. Eng.* **2019**, 2474370 (2019).
18. Xin, D., Study on Restriction Policy of Halon fire extinguishing agent for civil aircraft. *Scientific and technological horizon.* **08**, 257-227 (2017).
19. Oh, Y. J. M. J. Study on the promotion of recycling of old fire extinguishers. *Fire Sci. Eng.* **33**, 156 (2019).
20 Chernysheva, A. A., Lekhtmets, V. L. & Toleshov, A. K. Method of extending the service life of fire-extinguishing powders. *Metallurgist* **52**(3), 207–209 (2008).
21. Jong-Sang Kim, Y. H. Performance of recycled fire-extinguishing agents in terms of fire-fighting performance management. *Fire Sci. Eng.* **5**, 34 (2020).
22 Oh, J., Jang, S. G. & Yoh, J. J. Towards understanding the effects of heat and humidity on ageing of a NASA standard pyrotechnic igniter. *Sci. Rep.* **9**, 10203 (2019).
23 Jiang, F. X., Li, X. H., Li, P. X., Chen, S. Z. & Sun, Y. Life prediction of thermal aging of adhesive for retard-bonded prestressed tendons. *J. Appl. Polym. Sci.* **140**, e54623 (2023).
24 Yan, X., Guo, J. H. & Jiang, X. H. The microwave-absorption properties and mechanism of phenyl silicone rubber/CIPs/graphene composites after thermal-aging in an elevated temperature. *Sci. Rep.* **12**, 4385 (2022).
25. Sunny, J., Nazaripoor, H., Palacios Moreno, J. & Mertiny, P. Accelerated zero-stress hydrothermal aging of dry e-glass fibers and service life prediction using arrhenius model. *Fibers* **11**, 70 (2023).
26. Zhang, G. et al. Energetic, bio-oil, biochar, and ash performances of co-pyrolysis-gasification of textile dyeing sludge and Chinese medicine residues in response to K_2CO_3, atmosphere type, blend ratio, and temperature. *J. Environ. Sci.* **136**, 133 (2024).
27. Zhang, Y., Wang, Z., Li, Q., Pan, R. & Zhou, X. A novel approach for enhancing fire suppression efficiency of dry powder extinguishant: From the synergistic effect of dawsonite. *Powder Technol.* **431**, 119052 (2024).

28. Liu, Y., Chen, R., Guo, S., Wang, Z. & Pan, R. Modification and application performance study of ultra-fine dry powder extinguishing agent. *Molecules* **29**(16), 3830 (2024).
29. Wang, X. Study on modification technology of superfine dry powder fire extinguishing agent. *J. Phys.: Conf. Ser.* **2539**, 12091 (2023).
30. Shailesh Joshi, S. K. V. B. Quantitative analysis of sodium carbonate and sodium bicarbonate in solid mixtures using fourier transform infrared spectroscopy (FT-IR). *Appl. Spectrosc.* **67**, 841 (2013).
31. Liu, Y. et al. High-temperature oxidation and hot corrosion behaviors and mechanism of one typical aero-engine material 0Cr18Ni9 by one novel superhydrophobic and oleophobic ultrafine dry powder extinguishing agent. *J. Mater. Eng. Perform.* **24**, 14403 (2023).
32 Santos, T. et al. Effects of UV sensitivity and accelerated photo-aging on stab resistance of p-aramid fabrics impregnated with shear thickening fluids (STFs). *Heliyon* **9**, e15020 (2023).
33. Santos, T. F., Santos, C. M., Rangappa, S. M., Siengchin, S. & Nascimento, J. H. O. Statistical approach on the inter-yarn friction behavior of the dual-phase STF/ρ-Aramid impregnated fabrics via factorial design and 3D-RSM. *Heliyon* **9**, e18805 (2023).
34. Sengupta, A., Malik, S. N. & Bahadur, D. Developing superhydrophobic and oleophobic nanostructure by a facile chemical transformation of zirconium hydroxide surface. *Appl. Surf. Sci.* **363**, 346 (2016).

Acknowledgements

This work was sponsored by Hong Kong Scholars Program (No. XJ2021025), National Natural Science Foundation of China (No. 52276119), the Fundamental Research Funds for the Central Universities (No. 30922010909), China Postdoctoral Science Foundation (No. 2020M680069) and Jiangsu Planned Projects for Postdoctoral Research Funds (No. 2020Z414).

Author contributions

Yurong Liu: Conceptualization, data collection, methodology, writing original draft; Ruiyu Chen: Conceptualization, formal analysis, investigation, funding acquisition, project administration, supervision; Zhixuan Wang, Rui Zhang,Hongling Jing, Daheng Yu: Data collection, writing, review & editing; Renming Pan: Funding acquisition, project administration, supervision.

Competing interests

The authors declare no competing interests.

Additional information

Supplementary Information The online version contains supplementary material available at https://doi.org/10.1038/s41598-025-87718-w.

Correspondence and requests for materials should be addressed to R.C. or R.P.

Reprints and permissions information is available at www.nature.com/reprints.

Publisher's note Springer Nature remains neutral with regard to jurisdictional claims in published maps and institutional affiliations.

Open Access This article is licensed under a Creative Commons Attribution-NonCommercial-NoDerivatives 4.0 International License, which permits any non-commercial use, sharing, distribution and reproduction in any medium or format, as long as you give appropriate credit to the original author(s) and the source, provide a link to the Creative Commons licence, and indicate if you modified the licensed material. You do not have permission under this licence to share adapted material derived from this article or parts of it. The images or other third party material in this article are included in the article's Creative Commons licence, unless indicated otherwise in a credit line to the material. If material is not included in the article's Creative Commons licence and your intended use is not permitted by statutory regulation or exceeds the permitted use, you will need to obtain permission directly from the copyright holder. To view a copy of this licence, visit http://creativecommons.org/licenses/by-nc-nd/4.0/.

© The Author(s) 2025